Applied Surface Science 421 (2017) 778–782

Contents lists available at ScienceDirect

Applied Surface Science

journal homepage: www.elsevier.com/locate/apsusc

Optical properties of graphene oxide and reduced graphene oxide determined by spectroscopic ellipsometry

Stefan Schöche[a], Nina Hong[a], Mohammadreza Khorasaninejad[b], Antonio Ambrosio[b,c], Emanuele Orabona[c], Pasqualino Maddalena[c], Federico Capasso[b,*]

[a] J.A. Woollam Co., Inc., 645 M Street, Suite 102, Lincoln, NE 68508, USA
[b] School of Engineering and Applied Sciences, Harvard University, 29 Oxford Street, Cambridge, MA 02138, USA
[c] CNR-SPIN and Dipartimento di Fisica, Università degli Studi di Napoli Federico II, Via Cintia, 80126 Napoli, Italy

ARTICLE INFO

Article history:
Received 1 August 2016
Received in revised form
30 December 2016
Accepted 5 January 2017
Available online 11 January 2017

Keywords:
Graphene oxide
Reduced graphene oxide
Few-layer graphene
Spectroscopic ellipsometry
Optical constants

ABSTRACT

We report the optical constants of graphene oxide and reduced graphene oxide determined by spectroscopic ellipsometry. The dynamic changes in optical properties and thickness of a drop-cast graphene oxide layer during reduction by long-term exposure to focused broad-band white light are monitored in situ. The anisotropic optical constants of the graphene oxide layer and the isotropically averaged optical constants of the reduced layer are precisely determined from a multiple-location analysis of spatially resolved data across the exposed location and a multiple-time-step analysis of the dynamic data, respectively. Observed inter-band transitions in the graphene oxide layer are discussed in relation to theoretical predictions for different coverage levels of the graphene oxide sheets with oxygen containing functional groups. The derived optical constants of the reduced graphene oxide layer are compared to reported values of graphene and thermally reduced graphene oxide.

1. Introduction

Local reduction of graphene oxide (GO) presents a potential route for fabrication of graphene-based electronic devices and filling of gaps in device structures with graphene [1,2]. GO consists of oxidized graphene sheets decorated with epoxy, hydroxyl, carbonyl, and other oxygen containing functional groups [3–5] and is therefore water-soluble and suitable for various deposition strategies [3]. Several methods to produce GO by oxidative treatment of graphite were developed [6–8]. The oxygen groups break the sp^2-bond network of the graphene sheets and convert the material from a conducting to an insulating state. Reduction of the GO layers restores the electronic properties of graphene. Partial reduction and exposure to certain chemicals allows control of optical properties, band gap, and conductivity of the material [1,9–12]. The most common routes for reduction of GO are chemical [1,4,13] and thermal treatment [14–16]. Alternative approaches using electrochemistry and electric fields have been reported [17,18]. Reduction by exposure to light opened up a pathway to locally induce the insulator to conductor transition by standard lithographic processes [19–23]. In this case, the deoxygenation reaction is caused by light absorption and the resulting temperature increase. A review of fabrication, reduction mechanisms, and defect healing methods can be found in Ref. [24].

The transition between the insulating GO and conducting graphene state is accompanied by a change in the optical properties of the material. Spectroscopic ellipsometry (SE) has been applied to study the optical constants of graphite [25], exfoliated graphene flakes [13,25,26], chemical vapor deposition grown graphene [27–29], epitaxial graphene on SiC [30–32], and few-layer graphene [33,34]. The obtained optical constants were explained by theoretical band structure calculations and accounting for excitonic contributions [25,35,36]. Comparison of the derived optical constants shows slight variations in dependence of the preparation method due to interactions between the graphene sheets and the underlying substrate structure as well as between multiple graphene layers. The band structure and thus optical properties of GO depend on the oxygen group coverage and are harder to predict than for graphene or graphite [11,12]. Consequently, the optical properties of the reduced GO (r-GO) vary between the different reduction methods depending on residual oxygen group coverage and defects within the carbon sheets. However, knowledge of the optical properties is essential for process monitoring in an industrial environment and comparison of theoretical predictions with

* Corresponding author.
E-mail address: capasso@seas.harvard.edu (F. Capasso).

http://dx.doi.org/10.1016/j.apsusc.2017.01.035
0169-4332/

experimental results. The optical properties of thick as well as few-layer GO and thermally reduced r-GO were studied over a limited spectral range using imaging SE [14]. The optical properties of few-layer GO and chemically reduced r-GO were characterized by SE [10], however, unreasonably high values for the optical constants of GO and r-GO were reported in that publication.

In this work, we report the optical properties of GO and r-GO as determined by spectroscopic ellipsometry over a wide spectral range. The anisotropic optical properties of thick drop-cast GO are precisely determined in a multiple-location analysis making use of the varied film thickness across the sample between 1500 nm and 2500 nm. A parameterized oscillator model is derived in order to compare observed absorption features with theoretically predicted inter-band transition energies for different coverage levels of the GO sheets with oxygen-containing functional groups. Long-term exposure of the sample to the focused broad-band white-light beam of the ellipsometer causes the reduction of the GO. The variation of the sample properties is monitored in situ. The simultaneous analysis of multiple time steps during the reduction process (multiple-time-step analysis) allows the accurate characterization of the isotropically averaged optical properties of r-GO and the layer thickness in dependence of the exposure duration. The obtained optical constants are compared to literature values for graphene and thermally reduced r-GO.

2. Experiment

A suspension of GO in water was prepared by applying the Hummers method to nanocrystalline graphite (graphene nanoplatelets) according to a procedure described in literature [37]. The details are outlined in Ref. [21]. A thick GO film was prepared by drop casting the GO suspension on a thick SiO_2 film on Si substrates with subsequent exposure to air until water evaporation was completed. Fourier-transform infrared spectroscopy revealed that hydroxyl and carbonyl groups are the dominant species of oxygen containing groups in the GO films [21]. SE measurements were performed over the spectral range between 193 nm and 1690 nm on a J.A. Woollam M-2000 spectroscopic ellipsometer. This instrument uses a combination of a quartz tungsten halogen lamp and a deuterium lamp to provide a broad-band white light beam over the respective spectral range. Focusing probes were used to reduce the beam diameter to 300 μm at the sample surface. For the long-term exposure experiment, the white light beam was directed onto the sample surface under an angle of incidence of 65° for about 20 h while data was taken continuously. Subsequently, spatially resolved data was obtained at angles of incidence of 55° and 65° around the exposed location on an area of 4 mm × 4 mm.

3. Theory

The materials investigated here are either optically isotropic or uniaxial with optical axis oriented parallel to the surface normal. In this situation, no mode conversion of light polarized parallel (p) to polarization perpendicular (s) to the plane of incidence or vice versa occurs and the standard ellipsometry formalism can be applied [38]. The standard ellipsometric parameters Ψ and Δ are defined by the ratio ρ of the complex valued Fresnel reflection coefficients

$$\rho = \frac{\tilde{r}_p}{\tilde{r}_s} = \tan\Psi \cdot \exp(i\Delta). \quad (1)$$

The SE data was analyzed by setting up a layer-stack model in the CompleteEASE analysis software including the Si substrate, the thick SiO_2 layer, the GO layer, and the r-GO layer. The light propagation within the entire sample stack is calculated using a 4 × 4 transfer matrix algorithm for multi-layer systems with plane-parallel interfaces similar to the formalism derived by Berreman [39]. A regression analysis (Levenberg-Marquardt algorithm) is performed where model parameters are varied until calculated and experimental data match as close as possible [40].

In order to perform the transfer matrix algorithm, the dielectric function tensor components of each sample constituent are needed as input. For a uniaxial material the dielectric function tensor is given in diagonal form

$$\varepsilon = \begin{pmatrix} \varepsilon_\perp & 0 & 0 \\ 0 & \varepsilon_\perp & 0 \\ 0 & 0 & \varepsilon_\parallel \end{pmatrix}, \quad (2)$$

with two independent components $\varepsilon_\perp$ and $\varepsilon_\parallel$ where "⊥" and "∥" denote polarization perpendicular and parallel to the sample surface normal, respectively. For optically isotropic materials, this tensor reduces to a complex scalar function ε which is related to the complex refractive index $\tilde{n} = n + ik$ by $\varepsilon = \tilde{n}^2$, where n is the refractive index and k is the extinction coefficient. The dielectric function tensor components can be given as tabulated values for each photon energy, as interpolation functions of certain node spacing (B-splines [41]), or can be modeled themselves by using parameterized, energy-dependent algebraic functions, the model dielectric functions (MDF) [40]. These MDF describe a specific physical process in the material such as an electronic inter-band transition and are combined in order to render the overall spectral shape of a material's dielectric function.

The isotropic dielectric function of the Si substrate was adopted from the database without further modification [42]. The refractive index of the SiO_2 layer was modeled using the Cauchy dispersion relation for transparent materials, $n = A + B/\lambda^2 + C/\lambda^4 - D\lambda^2$, where λ is the wavelength of the probing light beam. The optical constants of the GO layer were initially modeled using B-spline functions which were then used as reference for a parameterized MDF approach applying Gaussian and Lorentzian oscillator functions [40]. The r-GO optical constants were modeled using B-splines. A surface roughness layer was included in the model analysis which was modeled according to the Bruggeman effective medium approximation as a 50:50 mixture of void and GO [40].

4. Results and discussion

The optical constants of the thick SiO_2 were determined from a multi-sample analysis of four different measurements performed on an uncoated area of sample. The thickness for each measurement spot, the surface roughness, a non-uniformity parameter, and the Cauchy parameters were included in the regression analysis. The obtained optical constants were then fixed and adopted for analysis of the GO samples without further modification.

In order to determine the optical constants of the drop-cast GO, a multi-sample analysis with two different angles of incidence was performed for nine different locations selected from a larger data map. A representative data set for a single measurement location is shown in Fig. 1.

The data set is dominated by thickness interference oscillations within the thick SiO_2 layer and the GO layer indicating a mostly transparent spectral region for the GO above 600 nm. The onset of stronger absorption within the GO layer towards shorter wavelengths appears as dampening and vanishing of the amplitude of these oscillations.

An anisotropic dielectric function tensor model had to be applied in order to match experimental and model data. Generalized ellipsometry measurements for multiple in-plane sample orientations did not indicate any in-plane anisotropy. Therefore, a dielectric function tensor with optical axes oriented along the sample surface normal was assumed. For high-index materials with

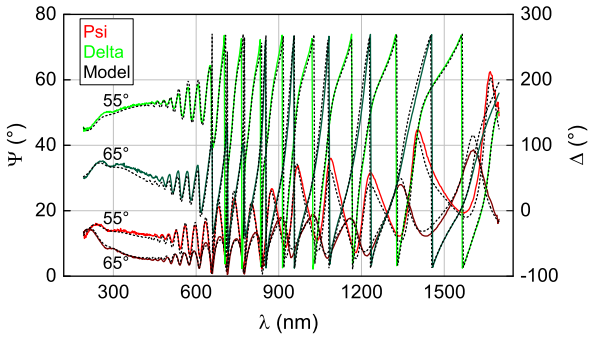

Fig. 1. Experimental (solid) and best-match model data (dashed) of the ellipsometric parameters Ψ (red) and Δ (green) for GO at a single measurement location. The best-match model data for a multi-sample analysis assuming a uniaxial dielectric function tensor model with optical axes parallel to the sample surface normal is shown.

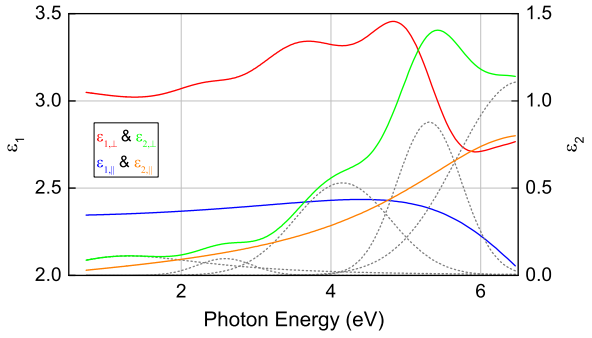

Fig. 3. Best-match model derived optical constants of GO using a set of MDF. Real (ε_1) and imaginary part (ε_2) of the dielectric function tensor components $\varepsilon_\perp$ and $\varepsilon_\parallel$ are shown as a function of photon energy. The individual oscillators forming $\varepsilon_{2,\perp}$ are indicated by dotted lines.

this optical axis orientation, very limited sensitivity to the out-of-plane optical constants (parallel to the sample surface normal) is expected [43]. Implying a similar shape of the in-plane and out-of-plane optical constants compared to graphite [25], $\varepsilon_\parallel = \tilde{n}_z^2$ is expected to be smooth without strong absorption over the entire measured spectral range. A Kramers–Kronig consistent B-spline layer with a wide node spacing of 1 eV was applied in order to model the respective dielectric function tensor component. The in-plane dielectric function tensor component $\varepsilon_\perp = \tilde{n}_x^2$ was modeled using a Kramers–Kronig consistent B-spline layer with a node spacing of 0.3 eV.

The thickness for each measurement spot, the surface roughness, a thickness non-uniformity parameter, and the B-spline nodes describing the imaginary part of the dielectric function tensor elements as well as constant offsets to the real parts of the dielectric function tensor elements were included in the regression analysis. The thickness non-uniformity parameter was included along with the angular spread and bandwidth of the detector array which were both fixed to nominal system parameters in order to account for depolarization effects. Measured depolarization data was analyzed along with the standard SE data to avoid systematic errors of the reported parameters and optical constants due to those effects.

The anisotropic model resulted in excellent match between experimental and model data which indicates a preferential orientation of GO sheets parallel to the sample surface in our drop-cast films. Film thicknesses between 1500 nm and 2500 nm were determined for the selected measurement spots. Thickness non-uniformity parameter values between 0% and 2.5% were observed. The obtained optical constants (Fig. 2) mimic the line shape for graphite and graphene, but with reduced refractive index and extinction coefficient magnitude. The extra-ordinary refractive index component $\tilde{n}_z$ shows a broad absorption which increases towards shorter wavelengths but without any peaks in the measured spectral range. Compared to graphene or graphite the ordinary refractive index component $\tilde{n}_x$ ($\varepsilon_\perp = \tilde{n}_x^2$) shows additional absorption peaks at lower energies compared to the van-Hove singularity which describes the inter-band transition between the π and π^* band at the M-point of the graphene Brillouin zone [25].

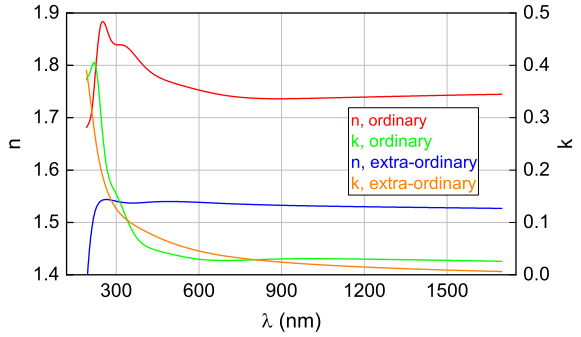

Fig. 2. Best-match model derived optical constants of GO using a B-spline set of optical constants. The ordinary ($\tilde{n}_x$) and extra-ordinary ($\tilde{n}_z$) complex refractive index $\tilde{n} = n + ik$ is shown as a function of wavelength λ.

In order to determine the position of the inter-band transitions in the GO layer, an MDF approach using a set of Gaussian and Lorentzian oscillators was chosen to match the B-spline optical constants. Three Gaussian oscillators within the measured spectral range and one Gaussian oscillator fixed at 6.5 eV describing strong absorption at higher photon energies outside the measured spectral range were combined to match the strong absorption features in $\tilde{n}_x$. An additional broad Lorentzian oscillator was included to describe the broad absorption in the NIR spectral range. The broad absorption feature in $\tilde{n}_z$ was matched using a single Lorentzian oscillator which was allowed to float to higher energies outside the measured spectral range. For both refractive index components, constant offsets to the real part of the dielectric function and a pole function to account for dispersion due to higher energy absorption outside the measured spectral range were included. The regression analysis was repeated with the replaced optical constants set. The resulting best-match model derived optical constants in terms of the dielectric function tensor components in dependence of the photon energy are presented in Fig. 3 and the obtained parameter set is summarized in Table 1.

Clearly separated absorption peaks in $\varepsilon_{2,\perp}$ appear at 5.31 eV, 4.15 eV, and 2.59 eV. A broad absorption peak at 1.88 eV has to be included in order to match the broad absorption feature in the NIR spectral range. Theoretical predictions by Johari and Shenoy [12] and by Boukhvalov et al. [11] suggest that the coverage level of the GO sheets with hydroxyl, epoxy, and carbonyl groups determines the energetic position of the $\pi \rightarrow \pi^*$ transition in GO. However,

Table 1
Summary of the best-matching model parameters obtained from the regression analysis for the parameterized GO model resulting in the optical constants shown in Fig. 3 with *A* denoting amplitude parameters, *B* broadening, and *E* center energies.

	Type	*A*	*B* (eV)	*E* (eV)
$\varepsilon_\perp$	Lorentz	0.09 ± 0.01	3.15 ± 0.17	1.90 ± 0.05
	Gauss	0.10 ± 0.01	0.87 ± 0.06	2.59 ± 0.04
	Gauss	0.53 ± 0.03	1.50 ± 0.16	4.15 ± 0.09
	Gauss	0.88 ± 0.08	1.02 ± 0.08	5.31 ± 0.03
	Gauss	1.11 ± 0.26	1.96 ± 0.33	6.5
	Pole	13.6 ± 1.8		7.55 ± 0.61
	ε_∞	2.18 ± 0.07		
$\varepsilon_\parallel$	Lorentz	0.79 ± 0.27	4.09 ± 0.75	6.90 ± 0.67
	ε_∞	1.88 ± 0.23		

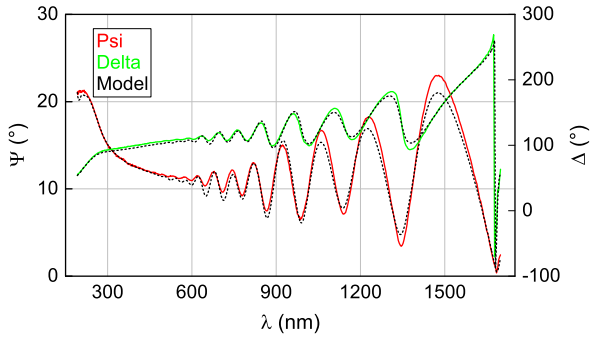

Fig. 4. Experimental (solid) and best-match model data (dashed) of the ellipsometric parameters Ψ (red) and Δ (green) for the GO sample after 20 h exposure to broad-band white light. The best-match model data for a multiple-time-step analysis assuming an isotropic dielectric function tensor model is shown.

certain distinct coverage levels are energetically favorable. Those configurations are illustrated in Refs. [11,12]. If epoxy and hydroxyl groups are present at the same time, a mixed coverage between 25% and 75% is energetically favorable [11]. In this case, both theoretical studies predict a strongly reduced energy for the $\pi \rightarrow \pi^*$ transition. Boukhvalov et al. predict an optical gap of 1.8 eV for a 50% coverage with epoxy and hydroxyl groups, and 2.3 eV for 75% coverage. For the same coverage level, Johari and Shenoy predict transition energies of 1.2 eV and 3.4 eV, respectively. For the pure case of coverage with only hydroxyl groups, Boukhvalov et al. predict optical gaps of 1.8 eV and 2.1 eV. It needs to be mentioned that both studies underestimate the $\pi \rightarrow \pi^*$ transition energy of pristine graphene. Since FTIR studies mainly identified the presence of hydroxyl and carbonyl groups in our samples, most likely the transition energies at 1.88 eV and 2.59 eV in our sample can be assigned to the presence of GO sheets with coverage levels of hydroxyl groups between 50% and 75% [44]. Johari and Shenoy further studied the influence of the presence of carbonyl groups on the GO sheets. A linear decrease of the optical gap with increasing oxygen-to-carbon ratio from 4 eV to 0.3 eV for ratios between 0% and 37.5% are predicted. Considering the rescaling of the pristine graphene energy gap, we can assign the absorption peak at 4.15 eV in our sample to the presence of GO sheets with carbonyl groups resulting in oxygen-to-carbon ratios of at least 20%. Eda et al. also observed an absorption feature at 4.1 eV in optical absorption spectra of GO which was assigned to the presence of carbonyl groups [45]. The authors further observed strong absorption corresponding to the $\pi \rightarrow \pi^*$ at 4.5–5.5 eV. Our observed absorption peak at 5.31 eV falls in that range. Shen et al. assigned this transition to a low-energy plasma transition, however, in an optical experiment plasma excitation is not possible. It is therefore likely that this transition is either related to the presence of GO sheets with carbonyl groups resulting in low oxygen-to-carbon ratios or the presence of GO sheets completely oxidized with epoxy or hydroxyl groups, which was predicted by Johari and Shenoy to result in optical gaps larger than the pristine graphene $\pi \rightarrow \pi^*$ transition.

The reduction of the GO by exposure to broad-band white light was monitored in situ using the ellipsometer beam as the light source. Compared to the initial data obtained on the pristine GO (Fig. 1), the data set after 20 h of exposure (Fig. 4) shows an overall upward shift of the Ψ values and a decrease of the amplitude of the oscillation pattern in Δ which indicates the formation of a surface layer with strong absorption over the entire measured spectral range. Note, that the reduction rate of GO for exposure to the relatively low-intensity white-light ellipsometer beam is very small compared to the measurement time of only 3 s (see discussion below). Thus, the individual measurements for the mapping data obtained on the GO sample discussed above were not significantly

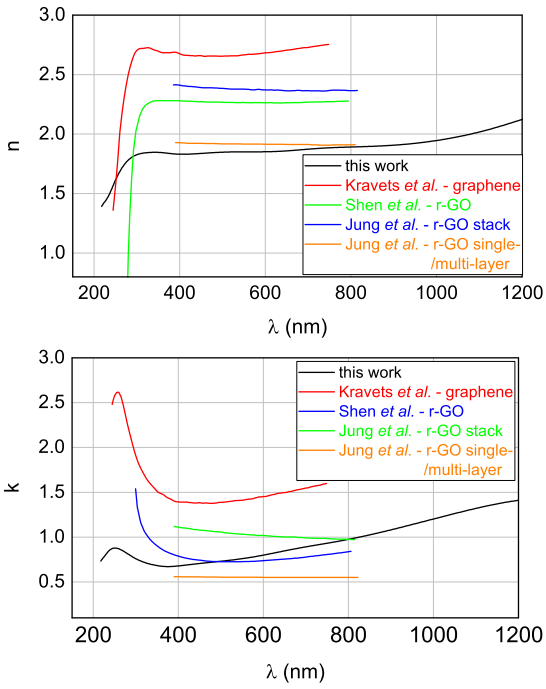

Fig. 5. Comparison of the obtained optical constants for r-GO to literature data of graphene and thermally reduced r-GO. The complex refractive $\tilde{n} = n + ik$ is shown for this work and data obtained from Refs. [10,14,25].

influenced by formation of a r-GO layer as confirmed by refitting the mapping data with a model in which the r-GO layer was included but resulted in vanishing thicknesses of that layer.

The simultaneous analysis of multiple time steps during the reduction process, under the assumption of equivalent optical properties while only the thickness of the reduced layer changes versus time, allows the precise determination of the layer optical properties even at very thin film thicknesses. An optical model assuming isotropic optical properties for the r-GO layer was applied to analyze single angle of incidence data of 20 time slices simultaneously. The graphene-like line shape of the r-GO optical constants was best matched using a B-spline approach. Additional model parameters varied during the regression analysis included the thickness of the GO and r-GO layers.

The best-match model result indicates a decrease of the GO thickness due to reduction from initially 1926.3 nm to 1828.1 nm within the 20 h of exposure while the r-GO layer thickness increased from 0 nm to 36.4 nm. The ratio between GO layer thickness decrease and r-GO layer thickness increase is about 2.7 while the ratio between the reported thickness of a single GO layer of 1 nm [3,5] and a single graphene sheet of 0.34 [25,26] is about 2.9 which might imply that not all functional groups were removed from the GO sheets during the reduction process, however, one should keep in mind that the thickness values reported here were determined with high precision and small correlation between thickness parameter values and optical constants since multiple time-slice data on many layers of GO and r-GO was investigated while the reported thicknesses for single-layer GO and graphene are likely not known as precisely.

The obtained optical constants for r-GO are shown in Fig. 5 in comparison to literature values for graphene and thermally reduced r-GO. The line shape of n and k clearly resembles the optical constants for graphene as reported in Ref. [25] with strong absorption towards long wavelengths indicating the conductive nature of the material and a single strong van-Hove singularity at about 250 nm. However, offsets compared to the graphene optical constants are observed. The values of the extinction coefficient k

is within the range of the values reported by Jung et al. for a stack of thermally reduced r-GO and single-/multilayer r-GO and the data reported by Shen et al. Nonetheless, our k values obtained for a multiple-time-step analysis of in situ data should be less influenced by correlation issues between thickness and optical constants than previously reported data and the line shape of the extracted optical constants appears more physically reasonable than for the previous reports. Our values of the refractive index n are found to be slightly lower than the values reported by others. Potential reasons might be an incomplete reduction of the GO sheets as indicated by the variation in the thickness discussed above and the potential incorporation of water between the sheets as suggested by other authors [14]. FTIR data obtained on samples exposed to green cw laser radiation for 15 min suggested the complete removal of hydroxyl groups while signatures of the carbonyl groups were still to be found in the data [21], which agrees with the shift of the highest energy transition in our data from 5.31 eV to 4.95 eV and the vanishing of the low energy absorption peaks. This result can be expected since carbonyl groups are bonded to the GO sheets by sp^2 hybridized bonds while hydroxyl and epoxy groups are bonded more weakly to sp^3 hybridized carbon atoms [12].

5. Conclusions

The anisotropic optical constants of GO were precisely determined from a multi-sample analysis of data obtained from a thick drop-cast layer. Uniaxial optical properties with optical axes oriented parallel to the sample surface normal were observed, indicating a preferential orientation of the GO sheets in the drop-cast sample parallel to the sample surface. An MDF model was derived in order to extract the energetic position of inter-band transitions in the GO layer due to the presence of oxygen containing groups. The observed transition energies were compared to theoretical predictions for specific coverage levels of the GO sheets with hydroxyl and carbonyl groups, which were found to be the dominant functional groups in our films by FTIR. The focused broad-band white-light beam of the ellipsometer was used in order to reduce the GO layer in a long-term exposure experiment while in situ data was obtained. A multiple-time-step analysis was performed in order to precisely determine the isotropically averaged optical constants of the reduced layer. A line-shape of the r-GO optical constants similar to graphene is observed, however, offsets in n and k are present. The observed ratio between the GO thickness decrease and the r-GO thickness increase as well as offsets of the optical constants compared to reported values for graphene suggest an incomplete reduction of our r-GO film which is in agreement with FTIR results. The obtained optical constants of the r-GO layer are comparable to previously reported values for r-GO, but the data presented in this work covers a wider spectral range, physically more reasonable line shapes were determined, and the simultaneous analysis of multiple-time-step data is expected to be less influenced by correlation effects between layer thickness and optical constants than for previous work on very thin films.

References

[1] G. Eda, Y.-Y. Lin, S. Miller, C.-W. Chen, W.-F. Su, M. Chhowalla, Appl. Phys. Lett. 92 (2008) 233305.
[2] G. Eda, G. Fanchini, M. Chhowalla, Nat. Nanotechnol. 3 (2008) 270–274.
[3] S. Stankovich, R.D. Piner, X. Chen, N. Wu, S.T. Nguyen, R.S. Ruoff, J. Mater. Chem. 16 (2006) 155–158.
[4] S. Stankovich, D.A. Dikin, R.D. Piner, K.A. Kohlhaas, A. Kleinhammes, Y. Jia, Y. Wu, S.T. Nguyen, R.S. Ruoff, Carbon 45 (2007) 1558–1565.
[5] M.J. McAllister, J.-L. Li, D.H. Adamson, H.C. Schniepp, A.A. Abdala, J. Liu, M. Herrera-Alonso, D.L. Milius, R. Car, R.K. Prud'homme, et al., Chem. Mater. 19 (2007) 4396–4404.
[6] B.C. Brodie, Philos. Trans. R. Soc. Lond. 149 (1859) 249–259.
[7] W.S. Hummers Jr., R.E. Offeman, J. Am. Chem. Soc. 80 (1958), 1339–1339.
[8] L. Staudenmaier, Ber. Dtsch. Chem. Ges. 31 (1898) 1481–1487.
[9] K.P. Loh, Q. Bao, G. Eda, M. Chhowalla, Nat. Chem. 2 (2010) 1015–1024.
[10] Y. Shen, P. Zhou, Q. Sun, L. Wan, J. Li, L. Chen, D. Zhang, X. Wang, Appl. Phys. Lett. 99 (2011) 141911.
[11] D.W. Boukhvalov, M.I. Katsnelson, J. Am. Chem. Soc. 130 (2008) 10697–10701.
[12] P. Johari, V.B. Shenoy, ACS Nano 5 (2011) 7640–7647.
[13] U. Wurstbauer, C. Röling, U. Wurstbauer, W. Wegscheider, M. Vaupel, P.H. Thiesen, D. Weiss, Appl. Phys. Lett. 97 (2010) 1901.
[14] I. Jung, M. Vaupel, M. Pelton, R. Piner, D.A. Dikin, S. Stankovich, J. An, R.S. Ruoff, J. Phys. Chem. C 112 (2008) 8499–8506.
[15] J. Lim, K. Choi, J. Rani, J.-S. Kim, C. Lee, J.H. Kim, S.C. Jun, J. Appl. Phys. 113 (2013) 183502.
[16] M. Acik, Y.J. Chabal, J. Mater. Sci. Res. 2 (2013) 101.
[17] S.Y. Toh, K.S. Loh, S.K. Kamarudin, W.R.W. Daud, Chem. Eng. J. 251 (2014) 422–434.
[18] S. Sahoo, G. Khurana, S.K. Barik, S. Dussan, D. Barrionuevo, R.S. Katiyar, J. Phys. Chem. C 117 (2013) 5485–5491.
[19] L.J. Cote, R. Cruz-Silva, J. Huang, J. Am. Chem. Soc. 131 (2009) 11027–11032.
[20] P. Kumar, K. Subrahmanyam, C. Rao, Int. J. Nanosci. 10 (2011) 559–566.
[21] E. Orabona, A. Ambrosio, A. Longo, G. Carotenuto, L. Nicolais, P. Maddalena, Opt. Lett. 39 (2014) 4263–4266.
[22] D.A. Sokolov, K.R. Shepperd, T.M. Orlando, J. Phys. Chem. Lett. 1 (2010) 2633–2636.
[23] Y. Zhou, Q. Bao, B. Varghese, L.A.L. Tang, C.K. Tan, C.-H. Sow, K.P. Loh, Adv. Mater. 22 (2010) 67–71.
[24] S. Pei, H.-M. Cheng, Carbon 50 (2012) 3210–3228.
[25] V. Kravets, A. Grigorenko, R. Nair, P. Blake, S. Anissimova, K. Novoselov, A. Geim, Phys. Rev. B 81 (2010) 155413.
[26] J. Weber, V. Calado, M. Van de Sanden, Appl. Phys. Lett. 97 (2010) 091904.
[27] M. Losurdo, M.M. Giangregorio, P. Capezzuto, G. Bruno, J. Phys. Chem. C 115 (2011) 21804–21812.
[28] F. Nelson, V. Kamineni, T. Zhang, E. Comfort, J. Lee, A. Diebold, Appl. Phys. Lett. 97 (2010) 253110.
[29] W. Li, G. Cheng, Y. Liang, B. Tian, X. Liang, L. Peng, A.H. Walker, D.J. Gundlach, N.V. Nguyen, Carbon 99 (2016) 348–353.
[30] A. Boosalis, T. Hofmann, V. Darakchieva, R. Yakimova, M. Schubert, Appl. Phys. Lett. 101 (2012) 011912.
[31] V. Darakchieva, A. Boosalis, A. Zakharov, T. Hofmann, M. Schubert, T. Tiwald, T. Iakimov, R. Vasiliauskas, R. Yakimova, Appl. Phys. Lett. 102 (2013) 213116.
[32] C. Bouhafs, V. Darakchieva, I. Persson, A. Tiberj, P.Å. Persson, M. Paillet, A.-A. Zahab, P. Landois, S. Juillaguet, S. Schöche, et al., J. Appl. Phys. 117 (2015) 085701.
[33] O. Albrektsen, R.L. Eriksen, S.M. Novikov, D. Schall, M. Karl, S.I. Bozhevolnyi, A.C. Simonsen, J. Appl. Phys. 111 (2012) 064305.
[34] G. Isić, M. Jakovljević, M. Filipović, D. Jovanović, B. Vasić, S. Lazović, N. Puač, Z.L. Petrović, R. Kostić, R. Gajić, et al., J. Nanophoton. 5 (2011) 051809.
[35] A. Matković, U. Ralević, G. Isić, M. Jakovljević, B. Vasić, I. Milošević, D. Marković, R. Gajić, Phys. Scr. 2012 (2012) 014069.
[36] D.-H. Chae, T. Utikal, S. Weisenburger, H. Giessen, K.V. Klitzing, M. Lippitz, J. Smet, Nano Lett. 11 (2011) 1379–1382.
[37] G. Carotenuto, V. Romeo, S. De Nicola, L. Nicolais, Nanoscale Res. Lett. 8 (2013) 1–6.
[38] M. Schubert, in: E.A. Irene, H.G. Tompkins (Eds.), Handbook of Ellipsometry, William Andrew Publishing, 2004.
[39] D.W. Berreman, J. Opt. Soc. Am. 62 (1972) 502.
[40] H. Fujiwara, Spectroscopic Ellipsometry: Principles and Applications, John Wiley & Sons Ltd., 2007.
[41] B. Johs, J.S. Hale, Phys. Status Solidi A 205 (2008) 715–719.
[42] C. Herzinger, B. Johs, W. McGahan, J. Woollam, W. Paulson, J. Appl. Phys. 83 (1998) 3323–3336.
[43] D. Aspnes, JOSA 70 (1980) 1275–1277.
[44] Note: the amplitude of the observed absorption peaks is not necessarily an indication for the fraction of sheets with certain coverage in our samples, since the absorption strength is determined by the joint density of states between π and π^* band, which will differ for the different oxidation states.
[45] G. Eda, M. Chhowalla, Adv. Mater. 22 (2010) 2392–2415.